Numerical Method for Homoclinic and Heteroclinic Orbits of Neuron Models

Bo Deng[1],[†]

Abstract A twisted heteroclinic cycle was proved to exist more than twenty-five years ago for the reaction-diffusion FitzHugh-Nagumo equations in their traveling wave moving frame. The result implies the existence of infinitely many traveling front waves and infinitely many traveling back waves for the system. However efforts to numerically render the twisted cycle were not fruitful for the main reason that such orbits are structurally unstable. Presented here is a bisectional search method for the primary types of traveling wave solutions for the type of bistable reaction-diffusion systems the FitzHugh-Nagumo equations represent. The algorithm converges at a geometric rate and the wave speed can be approximated to significant precision in principle. The method is then applied for a recently obtained axon model with the conclusion that twisted heteroclinic cycle maybe more of a theoretical artifact.

Keywords FitzHugh-Nagumo equations, twisted heteroclinic loop bifurcation, singular perturbation, bisection method.

MSC(2010) 34, 35, 37, 65, 92.

1. Introduction

The reaction-diffusion equations

$$\begin{cases} v_t = v_{xx} + f(v) - w \\ w_t = \epsilon(v - \gamma w) \end{cases} \tag{1.1}$$

with $f(v) = v(v-a)(1-v)$, $0 < a < 1/2$, $\gamma > 0$, $\epsilon > 0$, $t \geq 0$, $x \in \mathbb{R}$ was proposed by FitzHugh [1]and Nagumo [2] as a model for action potential impulses traveling along nerve axon. Researchers have been interested in the type of impulses which can be approximated by a fixed pulse profile but traveling at a constant speed. Such is a solution of one variable in the so-called moving frame: $(v, w)(t, x) = (V, W)(x + ct)$. Denote by $X' = \frac{dX}{dz}$ with $z = x + ct$. Then, $V(z), W(z)$ satisfy the following first order system of ordinary differential equations:

$$\begin{cases} V' = U \\ U' = cU - f(V) + W \\ W' = \frac{\epsilon}{c}(V - \gamma W) \end{cases} \tag{1.2}$$

[†]the corresponding author.

Email address:bdeng@math.unl.edu

[1]Mathematics, University of Nebraska-Lincoln, Lincoln, NE 68588, USA

A traveling impulse is a homoclinic orbit of the origin $(V, U, W) = \mathbf{0} = (0, 0, 0)$, satisfying

$$\lim_{z \to -\infty} (V, U, W)(z) = \mathbf{0} \quad \text{and} \quad \lim_{z \to \infty} (V, U, W)(z) = \mathbf{0}.$$

Most early studies in the literature were about such homoclinic solutions, c.f. [3–7].

When parameter γ is sufficiently large $\gamma > v_{max}/f_{max}$ (with $f_{max} = f(v_{max})$ and $v_{max} = [(a+1) + \sqrt{(a+1)^2 - 3a}]/3$ being the local maximal value of function f), the system has three equilibrium steady states which are on the plane $U = 0$, and on each branch of the cubic nonlinearity $W = f(V)$, separated by the critical points of the curve. The first is the origin $\mathbf{0}$ from which the impulse solution originates; the second is between the local minimal point v_{min} and the local maximal point v_{max} along the V axis which will not appear in our consideration from now on; and the third is above the local maximal point, denoted by $\mathbf{p} = (V_p, 0, W_p)$ with (V_p, W_p), being the solution to the equilibrium equation $W = f(V)$, $V = \gamma W$, which together with $\mathbf{0}$ are the focus of a few studies, including this one, in the literature. When the system is in this so-called bistable configuration, it is possible to have a front wave solution, corresponding to a heteroclinic orbit from $\mathbf{0}$ to $\mathbf{p}$:

$$\lim_{z \to -\infty} (V, U, W)(z) = \mathbf{0} \quad \text{and} \quad \lim_{z \to \infty} (V, U, W)(z) = \mathbf{p}.$$

Similarly a back wave solution may also exist, corresponding to a heteroclinic orbit from $\mathbf{p}$ to $\mathbf{0}$:

$$\lim_{z \to -\infty} (V, U, W)(z) = \mathbf{p} \quad \text{and} \quad \lim_{z \to \infty} (V, U, W)(z) = \mathbf{0}.$$

Traveling front and back waves were considered in [8–12]. In particular, Rinzel and Terman [9] studied the existence of a heteroclinic loop and its bifurcation to homoclinic orbits of both $\mathbf{0}$ and $\mathbf{p}$ for a closely related model to the FN equations.

The work of [13, 14] was the first to consider the effect of the orientation of the global stable manifolds in relation to the heteroclinic loop on the bifurcations of heteroclinic orbits other than the primary types forming the loop. The following result was obtained in Deng [14, 15]:

Theorem 1.1 (Theorem 1.1, [14], Theorem 2.3, [15])**.** *For each $0 < a < 1/2$ there is a sufficiently small $\epsilon_0 > 0$ and a fixed neighborhood $\mathcal{N} = (\gamma_1, \gamma_2) \times (c_1, c_2)$ of the point $\mathcal{B}_0 := (\gamma_0, c_0) = ((1 - 2a)/\sqrt{2}, 9/(2 - a)(1 - 2a))$ so that the following statements hold for every $0 < \epsilon < \epsilon_0$ and in $\mathcal{N}$ for system (1.2):*

1. *There are continuously differentiable curves $c = c_{f,0}(\gamma, \epsilon)$, $c = c_{b,0}(\gamma, \epsilon)$ satisfying at the singular limit $\epsilon = 0$:*

   $$c_{f,0}(\gamma, 0) = (1 - 2a)/\sqrt{2}, \quad c = c_{b,0}(\gamma, 0) = -(\beta_1 + \beta_3 - 2\beta_2)/\sqrt{2}$$

   for every $\gamma_1 < \gamma < \gamma_2$, where $\beta_1 < \beta_2 < \beta_3$ are the roots to the polynomial equation $-f(v) + W_p = 0$. Moreover, the two curves intersect at a point $(\gamma_\epsilon, c_\epsilon)$ with the properties that $(\gamma_\epsilon, c_\epsilon) = \mathcal{B}_0$ at $\epsilon = 0$, and the curve $c_{b,0}(\gamma, \epsilon)$ decreases through $c_{f,0}(\gamma, \epsilon)$ in γ at γ_ϵ.

2. *For each $\gamma_1 < \gamma < \gamma_2$, the system has a simple front wave at speed $c_{f,0}(\gamma, \epsilon)$ and a simple back wave at speed $c_{b,0}(\gamma, \epsilon)$. In particular, at $(\gamma_\epsilon, c_\epsilon)$ there is a heteroclinic loop from $\mathbf{0}$ to $\mathbf{p}$ and back to $\mathbf{0}$.*
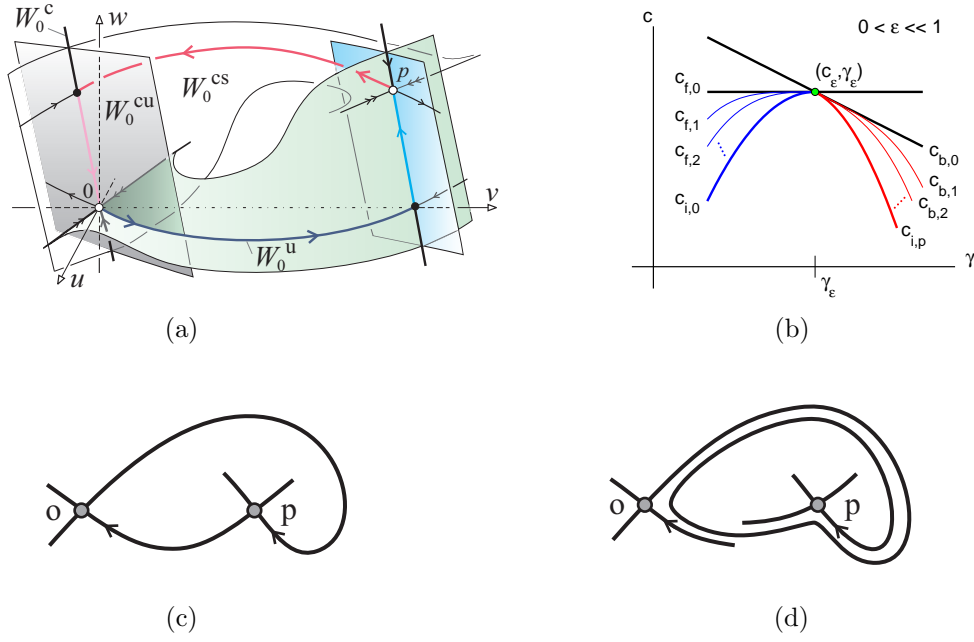
Figure 1. (a) Twisted heteroclinic loop of Eq.(1.2) at the singular limit $\epsilon = 0$. (b) Bifurcation diagram for the twisted loop for sufficiently small $0 < \epsilon \ll 1$. (c) A conceptual twisted heteroclinic loop on a plane. (d) A bifurcated heteroclinic orbit with one loop.

3. At the loop point $(\gamma_\epsilon, c_\epsilon)$, the **0**-**p** *heteroclinic orbit connects two different sides of the stable manifold of* **0** *and similarly, the* **p**-**0** *heteroclinic orbit connects two different sides of the stable manifold of* **p** *(with the limiting structure at $\epsilon = 0$ depicted as in Fig.1(a)).*

4. *There is a monotone decreasing sequence of differentiable functions $c = c_{f,n}(\cdot, \epsilon)$ on $(\gamma_1, \gamma_\epsilon)$, all asymptotically tangent to $c_{f,0}$ at the point $(\gamma_\epsilon, c_\epsilon)$. Also the sequence converges pointwise to a differentiable function $c = c_{i,0}(\cdot, \epsilon)$. Moreover, for each $\gamma \in (\gamma_1, \gamma_\epsilon)$ and $c = c_{f,n}(\gamma, \epsilon)$, the system has a* **0**-**p** *heteroclinic orbit which loops $n \geq 0$ times in a fixed neighborhood $\mathcal{H}$ of the heteroclinic cycle at (γ_0, c_0) and $\epsilon = 0$. For $c = c_{i,0}(\gamma, \epsilon)$, the system has a homoclinic orbit of* **0** *cycling only once in $\mathcal{H}$.*

5. *Similarly, there is a monotone decreasing sequence of differentiable functions $c = c_{b,n}(\cdot, \epsilon)$ on $(\gamma_\epsilon, \gamma_2)$, all asymptotically tangent to $c_{b,0}$ at the bifurcation point $(\gamma_\epsilon, c_\epsilon)$, and converging pointwise to a differentiable function $c = c_{i,p}(\cdot, \epsilon)$. And, for each $\gamma \in (\gamma_\epsilon, \gamma_2)$ and $c = c_{b,n}(\gamma, \epsilon)$, the system has a* **p**-**0** *heteroclinic orbit which loops $n \geq 0$ times in $\mathcal{H}$, and for $c = c_{i,p}(\gamma, \epsilon)$, the system has a homoclinic orbit of* **p** *cycling only once in $\mathcal{H}$.*

6. *For (γ, c) in the region of $\mathcal{N}$ below the homoclinic bifurcation curves $c_{i,0}$, $c_{i,p}$, the system has a periodic orbit looping only once in $\mathcal{H}$, i.e. a traveling train for (1.1).*

Figure 1 illustrates the structure of the twisted heteroclinic loop at the singular value $\epsilon = 0$ and the bifurcation diagram in the γc-parameter plane for each sufficiently

small $0 < \epsilon \ll 1$. It also gives an illustration on why a multiple-loop heteroclinic orbit can bifurcate from a twisted heteroclinic loop. Notice that without the twist no infinitely n-pulses front or back waves can bifurcate, see Deng [13].

As one consequence, one can see that since the speed parameter c is not a model parameter for the reaction-diffusion FN equations (1.1), the result above implies that for each γ near γ_ϵ, there are either infinitely many front waves or infinitely many back waves traveling at different speeds, c.f. Fig.1(b). This result naturally led to the question whether or not these infinitely many front and back waves are locally stable for the PDE (1.1)? Based on the manner by which the stable and unstable manifolds for the heteroclinic orbits break from each other when the speed parameter is perturbed and the Evans function used in [16, 17] for the linearization of the PDE at each of the front and back waves from the existence proof of the twisted loop, the stability was conjectured in [13], which was subsequently proved in [18–20].

In another direction, the question is how to render these orbits numerically for visualization. This is not a trivial problem it seems. For two dimensional Hamiltonian systems, this is usually done by plotting the level curves of the energy function. For higher dimensional systems or non-Hamiltonian systems, it is a hard problem because such orbits are highly unstable structurally. How to approximate them and how to control the numerical errors are continuous interests, c.f. [21–23]. The purpose of this paper is to illustrate a numerical method for neuron models that in effect turns a structurally diverging problem at some exponentially diverging rate into a numerically converging problem at some exponentially converging rate. The key idea is of bisectional search for solutions of scalar equations. Our approach is to use FNE as a test model to develop the method and to apply the method to a more realistic model.

2. Method and Result

Specifically, suppose finding a homoclinic or a heteroclinic orbit is reduced to finding a solution of an equation $h(x) = 0$ in an interval $x_1 < x < x_2$ with the property that $h(x_1) < 0 < h(x_2)$. Then we simply divide the interval into two equal halves, $x_1 < x_m < x_2$ with $x_m = (x_1 + x_2)/2$. In the next step, we define

$$x_1 = x_m \text{ if } h(x_m) < 0 \text{ and } x_2 = x_m \text{ if } h(x_m) > 0,$$

which gives rise to the new interval $[x_1, x_2]$ for the next iterative search. Let N be the total number of iterative steps and x^* be the right (or left) end point of the last output interval $[x_1, x_2]$ and x_0 be a solution of $h(x_0) = 0$ that is inside the last search interval. Then the error between the numerical approximation and the exact is of the order of $|x^* - x_0| \sim 2^{-N}$ with the proportionality being the initial interval length $x_2 - x_1$. With $N = 25$, 40, 50, the error order is respectively 10^{-8}, 10^{-12}, 10^{-16}. Namely, the approximation is accurate to, respectively, the 7th, 11th, 15th decimal place. For all the simulations below, we use $N = 40$ whenever a bisectional method is employed.

Also, the various bisectional methods to be presented below are very similar to each other for the type of reaction-diffusion equations represented by Eq.(1.1). The first, which is also the simplest, is for finding homoclinic orbits of Eq.(1.2).

2.1. Method for Homoclinic Orbit

On the outset, the goal is to find bounded solutions of the system, or equivalently, to exclude unbounded solutions, especially those on the unstable manifold of an equilibrium for homoclinic orbit. For the type of Eq.(1.2), we will exclude solutions which escape to infinity in variable V, doing so at a sufficiently high rate $|U| = |V'| \gg 1$. To this end, we define two exit planes, $U = U^+ \gg 1$ and $U = U^- \ll -1$. For the simulation implementation, we use $U^+ = 0.25$, $U^- = -0.25$.

We will limit parameter γ to a range so that $\mathbf{0} = (0, 0, 0)$ is the only equilibrium point of the system, satisfying $W = f(V)$, $V = \gamma W$, $U = 0$. For the simulation we use $\gamma = 5$, $a = 0.25$, $\epsilon = 0.003$. The shooting algorithm is to search the speed parameter c in an interval $[c_1, c_2]$ at a value c so that the system Eq.(1.2) has a homoclinic of the origin $\mathbf{0}$. The algorithm is as follows.

Bisectional Searching for Bounded Unstable Manifold (BSBUM):

1. For any given $c_1 \leq c \leq c_2$, compute the linearization of the vector filed at $\mathbf{0}$ using the first order discretization scheme for every partial derivative, $\frac{\partial F_i}{\partial x_j}(\mathbf{0}) \approx (F_i(\delta \mathbf{e_i}))/\delta$ where $\mathbf{e}_i$ is the standard basis vector with all entries zeros except for the ith entry which is the unit. For all numerical simulations $\delta = 10^{-16}$ is used.

2. Compute the stable and unstable eigenspaces E^s, E^u of the Jacobian $DF(\mathbf{0})$ from the previous step. We will restrict the tangent spaces to a small r-neighborhood of the equilibrium point $\mathbf{0}$ and use them as approximations to the local stable and local unstable manifolds, W^s_{loc}, W^u_{loc}. We know by a textbook fact that the error between the tangent plane approximation and the exact local manifold is of order r^2. For all numerical simulations $r = 10^{-5}$ is used. As a result, the approximation error for the stable and unstable manifolds is in the order of $r = 10^{-10}$.

3. For homoclinic orbit of the equilibrium point $\mathbf{0}$, we will take the branch of W^u_{loc} having positive U-component as the initial point to integrate it forward in time since an impulse profile in V increases first and then decreases. Matlab ODE solver `ode15s` for stiff systems is used with both the absolute error tolerance (`'AbsTol'`) and the relative error tolerance (`'RelTol'`) set at '1e-12' (10^{-12}). A typical solution which starts on the boundary of the r-neighborhood of $\mathbf{0}$ and ends on the exit planes $U = U^{\pm}$ usually takes less than 10^3 steps to complete. As a result, the total integration error is in the order of 10^{-9}. Denote by W^u the part of the global unstable manifold before hitting the exit planes $U = U^{\pm}$.

4. Initially, choose a parameter value $c = c_1$ so that by the method above W^u escapes through U^-, and similarly choose $c = c_2 > c_1$ so that W^u escapes through U^+. For the simulation, the initial interval is chosen to be $[c_1, c_2] = [0.2, 0.5]$.

5. The key step for the bisectional shooting algorithm is to compute the global unstable manifold W^u for the midpoint speed $c_m = \frac{c_1 + c_2}{2}$. The end points for the new searching interval is determined by the following bisection rule:

   $c_1 := c_m$, $c_2 := c_2$ if W^u exits $U = U^-$; and $c_1 := c_1$, $c_2 := c_m$ if otherwise.

6. The iteration is carried out for N steps. The c value at the last step is expected to be accurate roughly to the 11th decimal place. But due to the accuracies

(a)   (b)   (c)
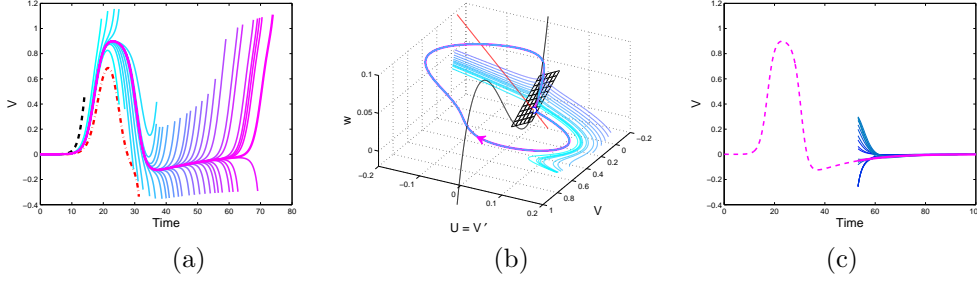
Figure 2. (a) Each trajectory corresponds to the unstable manifold of the trivial equilibrium point of Eq.(1.2) for the sequence of the speed parameter c generated by BSBUM. The trajectories which end pointing upward escape through the top exit plane $U = U^+$ and the others escape through the bottom exit plane $U = U^-$. Each type has the same slope at the end point. The dashed-curves correspond to the initial shooting speed parameters. (b) The grided parallelogram is the tangent plane of the local stable manifold, $T_0 W^s_{\mathrm{loc}}$, of the only equilibrium point **0**. Shooting orbits escape to infinity from either sides of the local stable manifold through the exit planes $U = U^+, U^-$, implying that the searched bounded orbit is a homoclinic orbit, (c) Each curve, except for the global unstable manifold trajectory, corresponds to an orbit on the stable manifold of the trivial equilibrium point, ending on the cross-section plane $W = w_0 = 0.01$ when initial points from the local stable manifold in a neighborhood of radius $r = 10^{-5}$ centered at the equilibrium **0** are integrated backward. The curves are the result of the bisectional shooting algorithm matching up the global unstable manifold (dash) with one orbit of the stable manifold (solid bold).

limited by other parts of the algorithm, we expect the speed value for the resulting bounded orbit to approximate the true value in the order of 10^{-9} at the least, an over estimate by the use of the Matlab solver.

Figure 2 is a demonstration of this searching algorithm for homoclinic orbit. In particular, Fig.2(a) shows the family of all unstable manifolds parameterized by the iterative speeds. All the V-profile curves pointing upward end with the slope $V' = U^+$ and all pointing downward end with the slope $V' = U^-$. Fig.2(b) shows the algorithm seeks out an homoclinic orbit of the system. Specifically, the grided plane at the origin is the tangent plane of the local stable manifold W^s_{loc} of **0** for the last c value that effectively directs the family of the unstable manifolds to either sides. As a result the numerically bounded solution the method seeks out is a homoclinic orbit, connecting the equilibrium point's unstable manifold to its stable manifold. The last loose end to tight up is to obtain a numerical homoclinic orbit which comes out from the r-neighborhood of the equilibrium and then returns to itself. The global unstable manifold W^u obtained by the bisectional shooting method about is only part of the homoclinic orbit because its closest returning distance to the origin is only of order 5×10^{-3}, far from the r-neighborhood with $r = 10^{-5}$. As a consequence, we need find a point from the local stable manifold W^s_{loc} from the r-neighborhood so that when integrated backward it meets the global unstable manifold W^u on a cross-section $W = w_0$. To stay far away from the part of W^u that has started to be expelled from the equilibrium point because of the instability of the equilibrium point due to the existence of the local unstable manifold, we will choose a fairly large value for w_0. Specifically, we will take $w_0 = 0.01$ for the homoclinic orbit. Again, we will use a bisectional search method to match the global unstable manifold and the global stable manifold on the cross-section $W = w_0$ as follows. We denote below the intersection of the global unstable manifold with the cross-section as $W^u \cap \{W = w_0\} = \{(V_0, U_0, w_0)\}$.

Bisectional Matching of Stable and Unstable Manifolds (BMSUM):

1. Consider one line segment on the tangent plane E^s of the local stable manifold W_{loc}^s on $W = r = 10^{-5}$, and parameterize the segment by a parameter s. For each s, integrate the corresponding stable manifold orbit backward to meet the cross-section $W = w_0$, and denote the intersection by (v_s, u_s, w_0). Denote also the displacement in the V-direction between the global manifolds by $d(s) = V_0 - v_s$. The goal is to find s so that $d(s) = 0$.

2. Find two values $s_1 < s_2$ to form the initial bisectional search interval so that $d(s_1) < 0 < d(s_2)$.

3. Carry out bisectional search in 40 steps to find a numerical solution s to $d(s) = 0$.

Fig.2(c) illustrates the process and the result of the bisectional match. The matching error is $|d(s)| = 5.420851781762215 \times 10^{-7}$. Corresponding to the U-variable, the matching error is $1.946175840534473 \times 10^{-6}$. We also tested the effective decimal digit for the speed c. This is done by keeping its decimals to a given position to see its effect on the homoclinic orbit. It shows that there is no discernible difference for the homoclinic orbit in the phase space (not shown, more on this later for heteroclinic cycle's effective digits) if the decimals are kept up to the 11th place. Here are resulting initial values:

$$(0.827998911477971, 0.560603803549176, 0.011881836452815) \times 10^{-5}$$

for the unstable manifold to pair with

$$(-0.973640759733335, 0.099386723238672, 0.204784726526954) \times 10^{-5}$$

for the stable manifold of $\mathbf{0}$, whose eigenvalues are -0.3407, -0.1021, 0.6771.

By keeping track of all the numerical errors throughout the bisectional shooting and matching processes we can state the following result.

Numerical Proposition 1: *Within a margin of error in the order of 10^{-6}, Eq.(1.2) has a numerical homoclinic orbit of the equilibrium point $\mathbf{0}$ for parameter values $a = 0.25$, $\gamma = 5$, $\epsilon = 0.003$, and $c = 0.286619666889283$, up to the 11th decimal place.*

2.2. Method for Heteroclinic Orbit

We next consider a moderate range for parameter γ. Specifically, $\gamma \in [8, 12]$ for the remaining exposition. For this range for γ and $a = 0.25$ the system has three equilibrium points, with the left most in the v-direction being the origin $\mathbf{0} = (0, 0, 0)$ and the right most denoted by $\mathbf{p} = (V_p, 0, W_p)$ for Eq.(1.2). For each $8 \leq \gamma \leq 12$, the $\mathbf{p}$ equilibrium point is found by a bisectional search in 40 steps to solve this equation

$$h(v) := f(v) - v/\gamma = 0, \quad \text{in the interval } v_{\max} \leq v \leq 1$$

where $v_{\max}$ is the local maximum point of the cubic curve $w = f(v)$. The linearization of the vector field of Eq.(1.2) at $\mathbf{p}$ is computed similarly as is done at $\mathbf{0}$ above for homoclinic orbit. Now the method to find the $\mathbf{0}$-$\mathbf{0}$ homoclinic orbit (impulse wave) above can be easily adapted to obtain the $\mathbf{0}$-$\mathbf{p}$ heteroclinic orbit (front wave) and the $\mathbf{p}$-$\mathbf{0}$ heteroclinic orbit (back wave). A few simple modifications are (a) for the $\mathbf{0}$-$\mathbf{p}$ heteroclinic orbit, the exit planes are $U = U_0^+ = 0.25$, $U = U_0^- = -0.01$ for finding
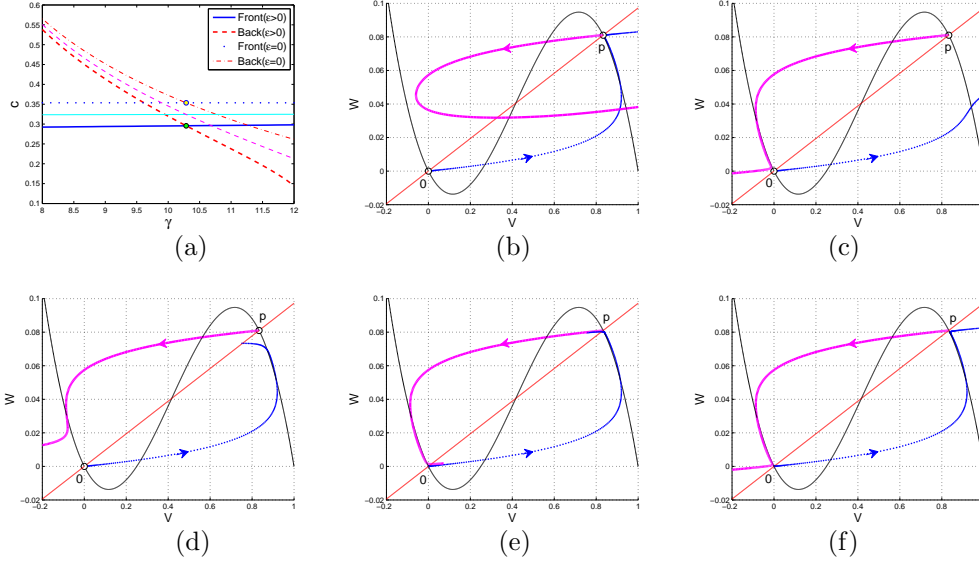
Figure 3. (a) Bifurcation diagram for the front and back waves of Eq.(1.2). The curves for $\epsilon = 0$ are exact, given by part (1) of Theorem. The other curves are for $\epsilon = 0.0016$, 0.003, respectively, with the latter for the thicker curves. (b) The unstable manifolds of the two equilibrium points **0**, **p** are shown for the parameter values from the discretized bifurcation curve $c_{f,0}$ that is nearest the intersection of the interpolated intersection, $(\gamma^*, c^*) = (10.285774076269378, 0.295700502206311)$, of the front and the back bifurcation curves, $c_{f,0}$, $c_{b,0}$. (c) The same type plot at (b) except for the nearest value from the back bifurcation curve $c_{b,0}$. (d) The same type of plot as (b,c) except at the interpolated values $\gamma = \gamma^*$ $c = c^*$. (e) The same type of plot except at the parameter values obtained by AHDBM with 40 steps. The resulting values are $\gamma_d = 10.285714184392418, c_d = 0.295700471139480$. (f) The same type of plot at the parameter values obtained by BBM with 40 steps bisection of the initial γ parameter interval $[8, 12]$. The resulting values are $\gamma_b = 10.285714185542020, c_b = 0.295700432794638$. The other parameter values are $a = 0.25$, $\epsilon = 0.003$ for all simulations.

a bounded unstable manifold W_0^u of **0**; (b) for the **p-0** heteroclinic orbit, the exit planes are $U = U_p^+ = 0.01$, $U = U_p^- = -0.25$ for finding a bounded unstable manifold W_p^u of **p** ((4) of BSBUM). The implementation parameters, r, δ, N, c_1, c_2, are the same as for the implementation of BSBUM above.

For the primary heteroclinic bifurcation curves $c_{f,0}$, $c_{b,0}$, we use 41 equally spaced discretization points for the γ-parameter interval $[8, 12]$. For each point γ_i, the bisectional method finds two speed values, one is for the simple front wave $c_{f,0}(\gamma_i, \epsilon)$ and the other is for the simple back wave $c_{b,0}(\gamma_i, \epsilon)$. These bifurcation curves, $c = c_{f,0}(\cdot, \epsilon)$, $c = c_{b,0}(\cdot, \epsilon)$, are plotted in Fig.3(a). It contains the ones with $\epsilon = 0$ which is done by the formula in part (1) of Theorem, and those with $\epsilon = 0.0016$, 0.003 which are done by the bisectional searching method. It shows that for each fixed $\epsilon \in [0, 0.003]$, the two curves cross each other transversally at a point $(\gamma_\epsilon, c_\epsilon)$, giving rise to a bifurcation point of heteroclinic cycle.

2.3. Methods for Heteroclinic Cycle

There are various ways to find numerical approximation to the heteroclinic loop bifurcation point (HLBP). We will start with the lest effective one. To this end, we consider the displacement function between the front and back bifurcation curves

as a function of parameter γ:

$$c = \phi(\gamma) := c_{b,0}(\gamma, \epsilon) - c_{f,0}(\gamma, \epsilon), \tag{2.1}$$

dropping the reference to the singular parameter ϵ for ϕ since it is fixed for what follows. The goal is to find the solution

$$\phi(\gamma) = 0$$

for the HLBP, denoting it by γ_h the exact solution, dropping the reference to ϵ as well. An intuitive method is by the way of discretization. Specifically, let G be the number of partitioning subintervals for an interval, say $[g_2, g_2]$, around γ_h. Denote by γ_i, $i = 0, 1, 2, \ldots, G$ the discrete points of partition. For $\epsilon = 0.003$, $G = 40$, and $[g_1, g_2] = [8, 12]$, Fig.3(b,c) show the nearest point approximation of γ_i to γ_h. It shows this approximation does poorly always to one of the two heteroclinic orbits.

The second method is by linear interpolation. That is, find the nearest points on both sides of γ_h and approximate γ_h by interpolation. Specifically, find i so that $\phi(\gamma_i) > 0$ and $\phi(\gamma_{i+1}) < 0$, and then find the intersection, denoted by (γ^*, c^*), of the lines through the ith and the $(i+1)$st points on $c_{f,0}$ and $c_{b,0}$. Using (γ^*, c^*) as an approximation of HLBP, Fig.3(d) shows the loop in the phase space. Comparing to the nearest point approximations, it has a better overall appearance for the loop but each connection is worse off than the best one by the nearest approximations. The follow-up question is will it become better by including more points to the discretization? Although the answer is affirmative but the rate of improvement is poor. Specifically, the approximation error is only improved linearly with respect to the reciprocal of the step size $\sim 1/G$. The reason is because the error function ϕ decreases transversely through γ_h with a nonzero slope, as it is shown by the bifurcation diagram Fig.3(a). As a result, if we double the points of discretization, we only expect to half the error. This is exactly what happened by our simulations. (For example, for the γ parameter, with $G = 40$, the error against the next better approximation (to be explained below) is $0.598918769600942 \times 10^{-4}$, and with $G = 80$, the same type error is $0.247911361377362 \times 10^{-4}$.) The conclusion is this interpolation method is not an effective method for HLBP because except for the points near the exact point all the other points contribute little to the accuracy of the approximation. (For comparison among various methods on the number of calls to the Matlab ODE solver, we use $G = N$ throughout.)

The next method is an *ad hoc* method, which works better than the previous methods but is not consistently reliable. Its performance depends on a few *ad hoc* factors we do not fully understand. The implementation parameters given below are the ones with which the method works well. For other choices, the result is ordinary. The method is a bisectional search carried out simultaneously on two parameters, γ and c. It works as follows.

Ad Hoc Double Bisection Method (AHDBM):

1. Find one interval each for parameters γ, c, $g_1 \leq \gamma \leq g_2$ and respectively $c_1 \leq c \leq c_2$, with the following properties: (i) For $\gamma = \frac{g_1 + g_2}{2}$, the unstable manifold of $\mathbf{0}$ corresponding to $c = c_1$ and $c = c_2$ exits through the plane $U = U_0^- = -0.01$, respectively, $U = U_0^+ = 0.25$. (ii) For $c = \frac{c_1 + c_2}{2}$, the unstable manifold of $\mathbf{p}$ corresponding to $\gamma = g_1$ and $\gamma = g_2$ exits through the plane $U = U_p^+ = 0.01$, respectively, $U = U_p^- = -0.25$.

2. For $c = \frac{c_1+c_2}{2}$ and $\gamma = \frac{g_1+g_2}{2}$, compute the global unstable manifold W_0^u of **0** and the global unstable manifold W_p^u of **p**. Define c to be the new c_1 iff W_0^u exits through $U = U_0^-$. Similarly, define γ to be the new g_1 iff W_p^u exits through $U = U_p^+$.

3. Repeat the process for N times.

For the parameter values $a = 0.25$, $\epsilon = 0.003$, the simulation presented here uses $[g_1, g_2] = [8, 16]$, $[c_1, c_2] = [0.25, 0.35]$ for the initial search intervals, and for a total of $N = 40$ steps. Fig.3(e) shows the global unstable manifolds W_0^u, W_p^u at the last step of the AHDBM. The Matlab solver `ode15s` was set to these values of controlling parameters: '1e-8' for both 'RelTol' and 'AbsTol', 'on' for 'BDF'. Notice that only $2N$ many calls to `ode15s` are made for this method.

This leads to the last method, combining the ideas of bifurcation and bisectional search. Recall the function $\phi(\gamma)$ from (2.1), the displacement function of the back bifurcation curve from the front bifurcation curve. We use bisection to find the solution of $\phi(\gamma) = 0$ on the interval $[g_1, g_2]$. In doing so at each step a given value γ, the algorithm computes first the front and the back bifurcation curves $c_{f,0}(\gamma, \epsilon)$, $c_{b,0}(\gamma, \epsilon)$ before determining the sign of $\phi(\gamma)$. Specifically, we have the following.

Bifurcational Bisection Method (BBM):

1. Set $\gamma = \frac{g_1+g_2}{2}$, and compute $\phi(\gamma)$, using $r = 0.00001$, $\delta = 10^{-16}$, $U = U_0^- = -0.01$, $U = U_0^+ = 0.25$ for the exit planes for the unstable manifold of **0**, and $U = U_p^+ = 0.01$, $U = U_p^- = -0.25$ for the exit planes for the unstable manifold of **p**.

2. Set γ to be the new g_1 iff $\phi(\gamma) > 0$.

3. Iterate the process for N times or terminate the search if the new ϕ value is greater than the one from the previous step and if both are of the same sign.

Fig.3(f) shows the result for $N = 40$ and the initial interval $[g_1, g_2] = [8, 12]$ and the initial speed interval $[c_1, c_2] = [0.1, 0.6]$ for every search for $c_{f,0}$, $c_{b,0}$. Since each bisectional search for the front and back speeds calls the Matlab ODE solver `ode15s` N times, the total number of such calls is in the order of $2N \times N$, the same number as for the nearest point interpolation method if $G = N$. The point (γ_b, c_b) is expected to be accurate at least to the 8th decimal place (the bisectional matching affects only the accuracy of the orbits in the phase space), much better than the nearest point interpolation method, and more consistently reliable than AHDBM.

To visualize the heteroclinic loop in the phase space, we can use BMSUM to match up the unstable manifold of one equilibrium to the stable manifold of the other. With the same implementation parameters the matching error is of the order of 10^{-6} on two cross-sections, 0.005 displacement in the W direction from the equilibrium points. Fig.4(a,b,c) show both AHDBM and BBM simulations, the matching, and the finished heteroclinic loop. Fig.4(d,e,f) also show the effective decimal digits for the parameter values γ_b, c_b by BBM. It shows that BBM's effective order of accuracy can be of 10^{-12}. Here are the initial points found by the methods:

$$(0.826307053570776, \ 0.563118860237200, \ 0.010667823786521) \times 10^{-5}$$
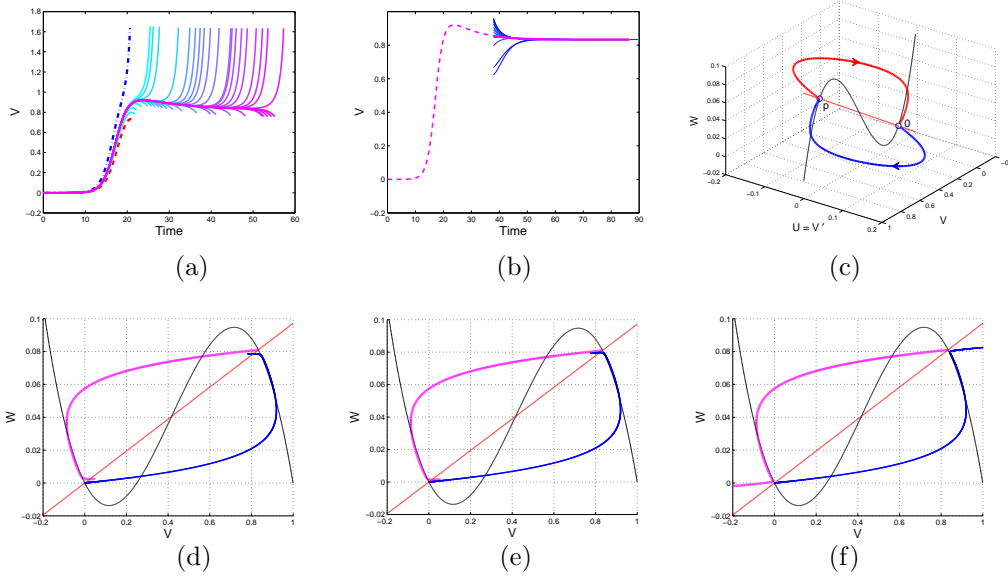
Figure 4. (a) AHDBM generated simple front wave. Dashed curves corresponding to the initial searching unstable manifolds of the equilibrium point **0** for two different speed parameters, $c_1 < c_2$ with $\gamma = (g_1 + g_2)/2$. Simultaneously, the back is searched (not shown) with the initial values $g_1 < g_2$ with $c = (c_1 + c_2)/2$. (b) The global unstable manifold from **0** from BBM is matched up to the stable manifold of **p** by the same BMSUM as for Fig.2(b) on cross-section $W = W_p - w_0$ with $w_0 = 0.005$. The same is done for the back wave (not shown) on the cross-section $W = w_0$. (c) The finished heteroclinic loop in the phase space. (d) The approximated heteroclinic loop by keeping the first 10 decimal digits of each parameter value $\gamma_b = 10.285714185542020$, $c_b = 0.295700432794638$ from BBM. (e) The same plot by keeping the first 11 decimal digits. (f) The same plot by keeping the first 13 decimal digits. Compare these to Fig.3(f) when no decimal digits of γ_b, c_b are dropped.

for the unstable manifold of **0** to pair with

$$(0.834492362203881, \ -0.000218598815839, \ 0.080799817752526)$$

for the stable manifold of $\mathbf{p} = (0.8333, \ 0, \ 0.0810)$, and

$$(0.833325124012760, \ -0.000005712385775, \ 0.081018403166356)$$

for the unstable manifold of **p** to pair with

$$(-0.971912781779798, \ 0.157393926626783, \ 0.170966471616465) \times 10^{-5}$$

for the stable manifold of **0**. The eigenvalues at **0**, **p** are, -0.3281, -0.1621, 0.6815, and respectively, -0.3668, -0.1531, 0.6960, showing the twist of both front and back waves can be well-defined.

The last numerical demonstration is to show that each heteroclinic orbit is twisted with respect to the other, namely, each comes out and return to opposite sides of the global stable manifold of an equilibrium point that contains the other heteroclinic orbit. This is shown in Fig.5 where the global stable manifolds are generated by integrating a set of points backward that are near the heteroclinic orbits and on the respective local stable manifolds. As a result when all numerical analyses are considered we have obtained an *in silico* proof for the following proposition:
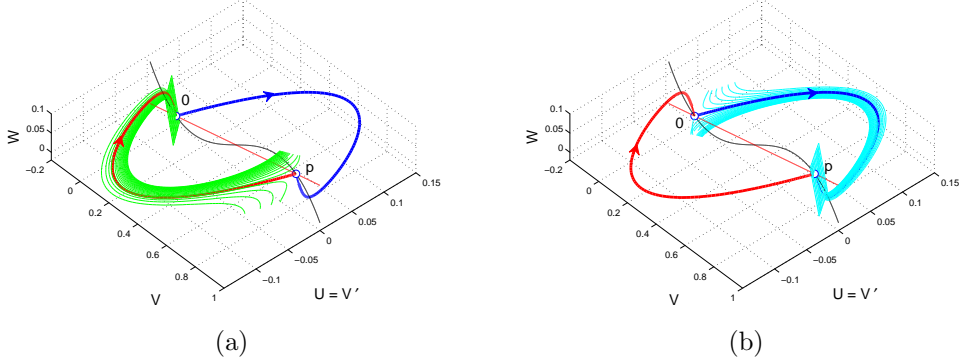
Figure 5. (a) The family of orbits forming the band are from the stable manifold of the equilibrium point **0**. The parallelogram is the tangent plane of the local stable manifold of **0** at the equilibrium point. Together they show one side of the stable manifold W_0^s of **0**. The **0**-**p** heteroclinic orbit (front wave) connects two different sides of W_0^s. (b) The same description as (a) except that the roles of **0** and **p** are reversed.

Numerical Proposition 2: *Within a margin of error in the order of* 10^{-6}, *Eq.(1.2) has a twisted heteroclinic cycle for parameter* $a = 0.25$, $\epsilon = 0.003$, $\gamma_b = 10.285714185542020$, *and* $c_b = 0.295700432794638$, *up to the 11th decimal place.*

This result says that within the margin of the error, what we have found by the method is indistinguishable from a twisted heteroclinic cycle. Equivalently, the exact orbit for the system with the parameter values can be something else entirely, but that may only be ascertained when all the errors are subject to a higher precision order.

3. Application

We now apply the ideas above to a mechanistic axon model obtained recently, Eq.(10) of [24]. It is as follows

$$
\begin{cases}
CV_t = DV_{xx} - [\bar{g}_{\mathrm{K}} n(V - E_{\mathrm{K}}) + \bar{g}_{\mathrm{Na}} m(V - E_{\mathrm{Na}}) + \bar{g}_{\mathrm{G}} h(V - E_{\mathrm{G}})] \\
n_t = \tau_{\mathrm{K}}(e^{(V - E_{\mathrm{K}})/b_{\mathrm{K}}} - n) \\
m_t = \tau_{\mathrm{Na}}(e^{(V - E_{\mathrm{Na}})/b_{\mathrm{Na}}} - m) \\
h_t = \tau_{\mathrm{G}}(e^{-(V - E_{\mathrm{G}})/b_{\mathrm{G}}} - h)
\end{cases}
\tag{3.1}
$$

Here, V is the intracellular membrane voltage, m, n, h are the dimensionless conductances for sodium, potassium and gating currents respectively, C is the membrane capacitance, D the axon diffusion parameter, E_{Na}, E_{K}, E_{G} the sodium, potassium, gating currents' resting potentials, $\bar{g}_{\mathrm{Na}}$, $\bar{g}_{\mathrm{K}}, \bar{g}_{\mathrm{G}}$ the sodium, potassium, gating channels' intrinsic conductances, b_{Na}, b_{K}, b_{G} the sodium, potassium, gating channels' activation range parameters, τ_{Na}, $\tau_{\mathrm{K}}, \tau_{\mathrm{G}}$ the sodium, potassium, gating conductances' adaptation-time parameters. Since the sodium and gating channels appear to activate first with a faster adaptation time than the potassium channel for the generation of action potentials, as a model simplification we can consider the slow Vn-system by taking the limit $\tau_{\mathrm{Na}}, \tau_{\mathrm{G}} \to \infty$ in the equations above to obtain

$m = e^{(V-E_{\mathrm{Na}})/b_{\mathrm{Na}}}$, $h = e^{-(V-E_{\mathrm{G}})/b_{\mathrm{G}}}$, and

$$\begin{cases} CV_t = DV_{xx} - \bar{g}_{\mathrm{K}}(V - E_{\mathrm{K}})(n - f(V)) \\ n_t = \tau_{\mathrm{K}}(e^{(V-E_{\mathrm{K}})/b_{\mathrm{K}}} - n) \end{cases} \tag{3.2}$$

where

$$f(V) = -[\bar{g}_{\mathrm{Na}}e^{(V-E_{\mathrm{Na}})/b_{\mathrm{Na}}}(V - E_{\mathrm{Na}}) + \bar{g}_{\mathrm{G}}e^{-(V-E_{\mathrm{G}})/b_{\mathrm{G}}}(V - E_{\mathrm{G}})]/[\bar{g}_{\mathrm{K}}(V - E_{\mathrm{K}})].$$

Similar to the FHN, we can introduce the traveling wave moving frame with speed c, $(V, n)(t, x) = (V, n)(z)$ with $z = x + ct$ and $U = V'(z)$ to have the corresponding traveling wave equations:

$$\begin{cases} V' = U \\ U' = [cCU + \bar{g}_{\mathrm{K}}(V - E_{\mathrm{K}})(n - f(V))]/D \\ n' = \tau_{\mathrm{K}}(e^{(V-E_{\mathrm{K}})/b_{\mathrm{K}}} - n)/c. \end{cases} \tag{3.3}$$

For a more numerically friendly version of the model, we scale the variables by $V := s_1 V$, $U := s_2 U$, $n := s_3 n$ with $s_1 = 70$, $s_2 = 200$, $s_3 = 300$. The dimensionless equations become

$$\begin{cases} V' = s_2 U/s_1 \\ U' = [cCs_2 U + \bar{g}_{\mathrm{K}}(s_1 V - E_{\mathrm{K}})(s_3 n - f(s_1 V))]/(s_2 D) \\ n' = \tau_{\mathrm{K}}(e^{(s_1 V - E_{\mathrm{K}})/b_{\mathrm{K}}} - s_3 n)/(s_3 c). \end{cases} \tag{3.4}$$

The qualitative similarities between this model and the FitzHugh-Nagumo equations lie in their nullclines. Specifically, the U-nullcline $n = f(V)$ on the V-nullcline surface $U = 0$ shapes like a letter N, and the n-nullcline $n = e^{(V-E_{\mathrm{K}})/b_{\mathrm{K}}}$ can easily intersect the former in a bistable configuration as shown in Fig.6(d). The similarity is more so if we treat the n-dynamics as slowly evolving, allowing the adaptation time parameter τ_{K} for the potassium conductance to be sufficiently small and turning it into a singularly perturbed system. As a result, the methods presented above can apply.

First, by BSBUM and BMSUM we obtained the following result for the model on impulse solution:

Numerical Proposition 3: *For the same parameter values as of [24] with $E_{\mathrm{K}} = -59.5$, $\bar{g}_{\mathrm{K}} = 0.0229$, $b_{\mathrm{K}} = 16.6$, $E_{\mathrm{Na}} = 67.5$, $\bar{g}_{\mathrm{Na}} = 100$, $b_{\mathrm{Na}} = 18.4$, $E_{\mathrm{G}} = -56$, $\bar{g}_{\mathrm{G}} = 9.3333$, $b_{\mathrm{G}} = 7.0667$, $C = 1$, $\tau_{\mathrm{K}} = 0.8667$, and $D = 1$, Eq.(3.4) has a numerical traveling wave solution of the equilibrium point $(-0.7455, 0, 0.0052)$ with wave speed $c = 2.856562267319505$ cm/msec up to the 11th decimal place. The eigenvalues of the linearization at the equilibrium point are -0.8088, -0.3058, 3.6678. The forward initial values for the wave are*

$$V_0 = -0.745445704516082, \ U_0 = 0.000007888895922, \ n_0 = 0.005180183446415$$

from the equilibrium point's unstable manifold and the backward initial values are

$$V_0 = -0.745455211292413, \ U_0 = 0.000000356972661, \ n_0 = 0.005189578595573$$

(a)

(b)

(c)

(d)
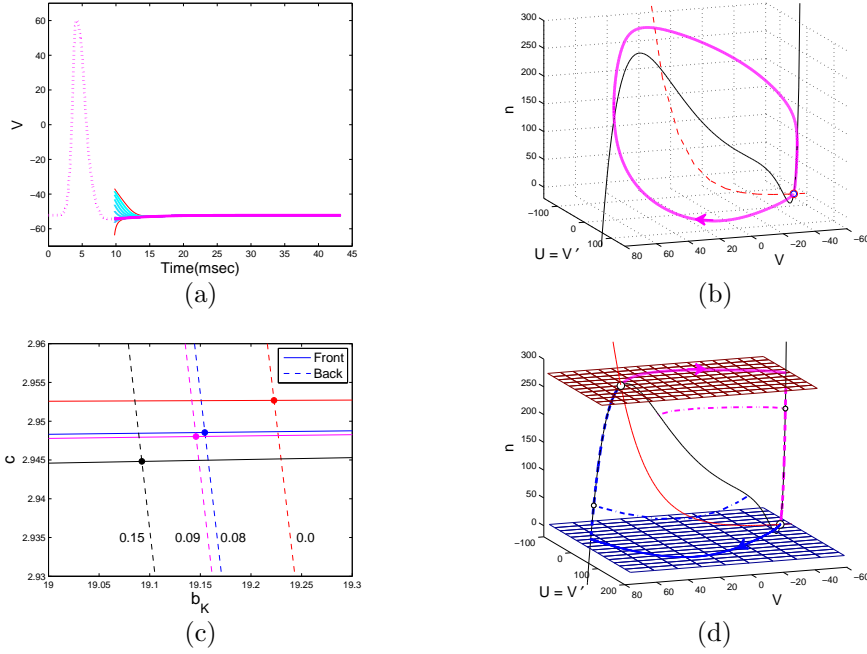
Figure 6. (a) It shows the matching of the unstable manifold to the stable manifold on the section $n = 0.4$ in V for impulse traveling wave of Eq.(3.4). (b) The impulse solution in the phase space, showing in addition the N-shaped U-nullcline $n = f(V)$ and the n-nullcline (dashed curve) on the V-nullcline surface $U = 0$. (c) Front and back bifurcation curves with different τ_{K} values next to the back curves. The intersection of each pair represents the existence of a heteroclinic loop. (d) The singular heteroclinic loop in the phase space for $\tau_{\mathrm{K}} = 0$. One orbit (dot-dash curve) from the center-stable manifold of each equilibrium point is shown, which all converge to the spiral equilibrium point in the middle branch of the N-shaped U-nullcline $n = f(V)$, indicating each singular heteroclinic orbit from one equilibrium point connects different sides of the center-stable manifold of the other equilibrium point. All plots are in the dimensional values of the variables.

from the stable manifold. The matching errors for V and U on the cross-section $n = 0.4$ are 0.000331402898996 and 0.000041476895305, respectively.

We note that except for the sodium and gating adaptation time constants, which are assumed to be the same and set to $\tau_{\mathrm{Na}} = \tau_{\mathrm{G}} = \infty$, the impulse solution is found for the parameter values fitted to Hodgkin-Huxley's experimental data (see [24]) with the speed value consistent with the result of Hodgkin and Huxley [25]. See Fig.6(a,b) for plots of the numerical orbit. Notice that unlike the FNE, the n-nullcline intersects the U-nullcline always at three points, creating the all-or-nothing firing configuration for the action potential impulse, consistent with empirical findings of nerve axons.

Next, we consider the existence of heteroclinic loops for the model, and more specifically, how far away from the fitted parameter values does such an orbit exist. We searched for them by BBM, with Fig.6(c,d) summarizing the result. Fig.6(c) shows the bifurcation diagram for the front bifurcation curve and the back bifurcation curve for four different values of the potassium adaptation time constant τ_{K}. At the singular value $\tau_{\mathrm{K}} = 0$, a singular heteroclinic loop is found for the same parameter values as for Fig.6(a,b) except for $b_{\mathrm{K}} = 19.222761097550393$ and $c = 2.952684300151825$. The bottom equilibrium (with low n value) is $(-0.7454, 0, 0.0049)$ with eigenvalues 3.7420, -0.7894, 0, and the top equilibrium is $(0.6912, 0, 0.9126)$
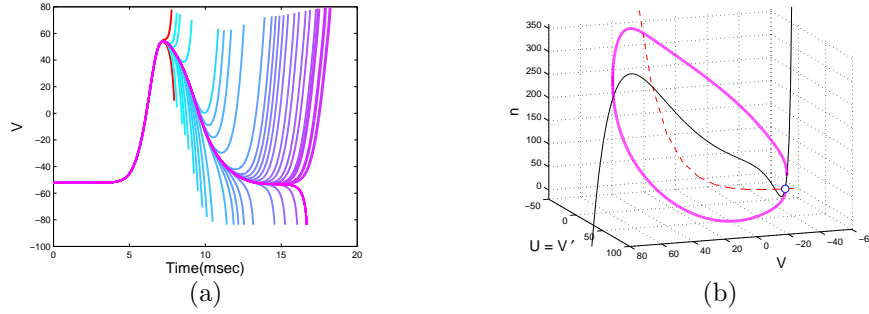
Figure 7. (a) Bisectional search of homoclinic orbit for the full model Eq.(3.5). (b) The orbit projected into the VUn-space. Because the local matching algorithm does work, the orbit is missing a piece on the local stable manifold of the resting equilibrium point.

with eigenvalues 4.1011, -1.1484, 0. Fig.6(d) shows the singular loop with the initial value for the front solution being

$$(-0.745372997141170, \ 0.000007948107972, \ 0.00487905548732)$$

and the initial value for the back solution being

$$(0.691203659413845, \ -0.000008205114823, \ 0.912613114307757).$$

Each is a VU-fast orbit lying on an $n =$ constant plane. The n-slow orbits lie on the left and right branches of the U-nullcline. The plot of one stable fiber for each branch of the center manifold also suggests that each singular heteroclinic orbit is twisted with respect to the other satisfying the conditions of Bell and Deng [15]. Our analysis also shows the heteroclinic loop can be continued to higher $\tau_{\kappa} < 0.5$ but not to the experiment-fitted value 0.8667. In addition, the twist of the loop cannot be continued beyond $\tau_{\kappa} = 0.09$ at which the stable eigenvalues of the top equilibrium point become a pair of complex numbers. For example, for $\tau_{\kappa} = 0.15$, the bottom equilibrium is $(-0.7454, 0, 0.0049)$ with eigenvalues 3.7434, -0.7984, -0.0512, and the top equilibrium is $(0.6819, 0, 0.9164)$ with eigenvalues 3.9278, $-0.5171\pm0.4833i$. Such eigenvalue conditions are well-known to create chaotic dynamics for homoclinic orbits (e.g. [26,27]). Furthermore, the heteroclinic loop bifurcation point is far from the experiment-fitted value in the range parameter value $b_{\kappa} = 16.6$. In fact, for $b_{\kappa} < 18.5$, the top equilibrium point lies on the middle branch of the N-shaped U-nullcline, destroying the bi-stability configuration for twisted heteroclinic cycle. As a consequence, heteroclinic cycle is not a realistic phenomenon for axon because the parameter values are far from the experiment-fitted values.

Last, the goal for developing the method above is to study the full mechanistic model Eq.(3.1). By casting it in the traveling wave moving frame and changing it to dimensionless form with scales $s_1 = 70$, $s_2 = 200$, $s_3 = 300$, $s_4 = 1$, $s_5 = 10$,

we obtain the following five-dimensional traveling wave equations

$$
\begin{cases}
V' = s_2 U / s_1 \\
U' = [cC s_2 U + \bar{g}_{\mathrm{K}} s_3 n(s_1 V - E_{\mathrm{K}}) + \bar{g}_{\mathrm{Na}} s_4 m(s_1 V - E_{\mathrm{Na}}) \\
\qquad\qquad + \bar{g}_{\mathrm{G}} s_5 h(s_1 V - E_{\mathrm{G}})] / (s_2 D) \\
n' = \tau_{\mathrm{K}} (e^{(s_1 V - E_{\mathrm{K}})/b_{\mathrm{K}}} - s_3 n) / (s_3 c) \\
m' = \tau_{\mathrm{Na}} (e^{(s_1 V - E_{\mathrm{Na}})/b_{\mathrm{Na}}} - s_4 m) / (s_4 c) \\
h' = \tau_{\mathrm{G}} (e^{-(s_1 V - E_{\mathrm{G}})/b_{\mathrm{G}}} - s_5 h) / (s_5 c).
\end{cases}
\tag{3.5}
$$

The resting potential equilibrium has one positive eigenvalue and four negative eigenvalues. As a result, BSBUM applies. However, because of the higher dimensionality for the stable manifold, the matching algorithm BMSUM does not work as is. Nonetheless, by using $U^+ = 1$, $U^- = -1$ and $c \in [2.123, 2.125]$ with BSBUM we can find a traveling wave solution and its speed as follows, see also Fig.7.

Numerical Proposition 4: *For the same parameter values as of [24] with $E_{\mathrm{K}} = -59.5$, $\bar{g}_{\mathrm{K}} = 0.0229$, $b_{\mathrm{K}} = 16.6$, $E_{\mathrm{Na}} = 67.5$, $\bar{g}_{\mathrm{Na}} = 100$, $b_{\mathrm{Na}} = 18.4$, $E_{\mathrm{G}} = -56$, $\bar{g}_{\mathrm{G}} = 9.3333$, $b_{\mathrm{G}} = 7.0667$, $C = 1$, $\tau_{\mathrm{Na}} = 10$, $\tau_{\mathrm{G}} = 10$, $\tau_{\mathrm{K}} = 0.8667$, and $D = 1.42$, Eq.(3.5) has a numerical traveling wave solution of the equilibrium point $(-0.7455, 0, 0.0044, 0.0015, 0.6711)$ with wave speed $c = 2.123808482768276$ cm/msec up to the 11th decimal place. The eigenvalues of the linearization at the equilibrium point are -5.1032, -4.7075, -0.7333, -0.4123, 2.6305. The initial point for the homoclinic orbit is $V_0 = -0.745451620653515$, $U_0 = 0.000000204576461$, $n_0 = 0.004440149175779$, $m_0 = 0.001496784986486$, $h_0 = 0.671107716136303$.*

We note that the wave speed was 2.12 cm/msec by Hodgkin-Huxley's experiment and 1.88 cm/msec by Hodgkin-Huxley's equations for their squid giant axons, see [25]. Heteroclinic loop can also be found for the full system by varying parameter b_{K}. But since the range has to be above and beyond the experiment-fitted value in order for the system to have a bi-stable configuration, such dynamics is probably not realistic. In addition, for example, with the same parameter values as above except for $b_{\mathrm{K}} = 19.2$, the linearization of the vector field at the equilibrium point with the higher n value has one positive eigenvalue and four eigenvalues of negative real part for the bi-stable configuration of a heteroclinic loop. But the stable eigenvalues that are nearest the imaginary axis is a pair of complex number under which the twist of a heteroclinic orbit cannot be defined. As a result we will skip the presentation of such orbits.

4. Closing Remarks

We have demonstrated for the type of FitzHugh-Nagumo reaction-diffusion equations a numerical method to find the primary types of traveling impulses, traveling front, and traveling back waves. The numerical scheme converges at exponential rate. The errors of approximation can effectively be controlled by keeping tracking of approximations to the local invariant manifolds, error tolerances of the Matlab ODE solver, and the matching errors between the global invariant manifolds. However, our method stops short at the problem of finding the homoclinic bifurcation curves $c_{i,0}, c_{i,p}$ and the n-pulse heteroclinic curves $c_{f,n}, c_{b,n}$ for $n \geq 1$. It is not

a natural extension of the current method to accomplish these goals because the required method has to first channel the family of unstable manifolds of one equilibrium point to avoid hitting the stable manifolds of the other equilibrium point, and to stay on one side of the stable manifolds of the other and/or of itself before connecting one member of the family to the stable manifold of the other equilibrium point or of itself, c.f. Fig.1(d). Nevertheless, the bisectional searching and matching ideas presented here should serve as a starting point and be part of the yet-to-complete strategy.

As for the mechanistic axon models Eq.(3.1), Eq.(3.2), action potential impulse solutions are also demonstrated for experiment-fitted parameter values, but the existence of heteroclinic cycles remains more of a theoretical curiosity than a probably phenomenon. However, a rigorous, singular perturbation proof for a twisted heteroclinic loop for the reduced model Eq.(3.4) and its stability should be an interesting mathematical problem which we shall leave it for another time.

Acknowledgement

References

[1] R. FitzHugh, *Impulses and physiological states in theoretical models of nerve membrane*, Biophysical Journal, 1961, 6(1), 445–466.

[2] J. Nagumo, S. Arimoto, and S. Yoshizawa, *An active pulse transmission line simulating nerve axon*, Proceedings of the IRE, 1962, 50(10), 2061šC-2070.

[3] H. P. McKean, *Nagumo¡s equation*, Advances in Mathematics, 1970, 4(3), 209-šC223.

[4] D. G. Aronson and H. F. Weinberger, *Nonlinear diffusion in population genetics, combus416 tion, and nerve pulse propagation*, Lecture Notes in Mathematics, 1975, 446, 5šC-49.

[5] S. Hastings, *On the existence of homoclinic and periodic orbits for the FitzHugh-Nagumo equations*, The Quarterly Journal of Mathematics, 1976, 27(1), 123šC-134.

[6] P. C. Fife and J. B. McLeod, *The approach of solutions of nonlinear diffusion equations to travelling front solutions*, Archive for Rational Mechanics and Analysis, 1977, 65(4), 335–361.

[7] J. W. Evans, N. Fenichel, and J. A. Feroe, *Double impulse solutions in nerve axon equations*, SIAM Journal on Applied Mathematics, 1982, 42(2), 219–234.

[8] G. A. Carpenter, *A geometric approach to singular perturbation problems with applications to nerve impulse equations*, Journal of Differential Equations, 1977, 23(3), 335–367.

[9] J. Rinzel and D. Terman, *Propagation phenomena in a bistable reaction-diffusion system*, SIAM Journal on Applied Mathematics, 1982, 42(5), 1111–1137.

[10] S.-N. Chow, B. Deng, and D. Terman, *The bifurcation of homoclinic and periodic or bits from two heteroclinic orbits*, SIAM Journal on Mathematical Analysis, 1990, 21(1), 179–204.

[11] H. Kokubu, Y. Nishiura, and H. Oka, *Heteroclinic and homoclinic bifurcations in bistable reaction diffusion systems*, Journal of Differential Equations, 1990, 86(2), 260–341.

[12] S.-N. Chow, B. Deng, and D. Terman, *The bifurcation of homoclinic orbits from two heteroclinic orbits–a topological approach*, Applicable Analysis, 1991, 42(3-4), 275–299.

[13] B. Deng, *The bifurcations of countable connections from a twisted heteroclinic loop*, SIAM Journal on Mathematical Analysis, 1991, 22(3), 653–679.

[14] B. Deng, *The existence of infinitely many traveling front and back waves in the FitzHugh-Nagumo equations*, SIAM Journal on Mathematical Analysis, 1991, 22(6), 1631–1650.

[15] D. C. Bell and B. Deng, *Singular perturbation of n-front travelling waves in the FitzHugh-Nagumo equations*, Nonlinear Analysis: Real World Applications, 2002, 3(4), 515–541.

[16] J. W. Evans, *Nerve axon equations: III stability of the nerve impulse*, Indiana University Mathematics Journal, 1972, 22(6), 577–593.

[17] C. K. Jones, *Stability of the travelling wave solution of the FitzHugh-Nagumo system*, Transactions of the American Mathematical Society, 1984, 286(2), 431–469.

[18] S. Nii, *Stability of travelling multiple-front (multiple-back) wave solutions of the FitzHugh-Nagumo equations*, SIAM Journal on Mathematical Analysis, 1997, 28(5), 1094–1112.

[19] B. Sandstede, *Stability of n-fronts bifurcating from a twisted heteroclinic loop and an application to the FitzHugh-Nagumo equation*, SIAM Journal on Mathematical Analysis, 1998, 29(1), 183–207.

[20] S. Nii, *A topological proof of stability of n-front solutions of the FitzHugh-Nagumo equations*, Journal of Dynamics and Differential Equations, 1999, 11(3), 515–555.

[21] J. Guckenheimer and C. Kuehn, *Homoclinic orbits of the Fitzhugh-Nagumo equation: The singular-limit*, Discrete and Continuous Dynamical Systems, Series S, 2009, 2(4), 851–872.

[22] K. Matsue, *Rigorous numerics for fast-slow systems with one-dimensional slow variable: topological shadowing approach*, arXiv preprint arXiv:1507.01462, 2015.

[23] A. Czechowski, *Rigorous numerics for a singular perturbation problem*, PhD thesis, dissertation, submitted, electronic version available at www.ii.uj.edu.pl/∼czechows, 2015.

[24] B. Deng, *Alternative models to Hodgkin-Huxley equations*, Bulletin of Mathematical Biology, 2017, 79(6), 1390–1411.

[25] A. L. Hodgkin and A. F. Huxley, *A quantitative description of membrane current and its application to conduction and excitation in nerve*, The Journal of Physiology, 1952, 117(4), 500–544.

[26] L. Shilnikov, *The existence of a denumerable set of periodic motions in four-dimensional space in an extended neighborhood of a saddle-focus*, in Soviet Math. Dokl, 1967, 8, 54–58.

[27] B. Deng, *On Shilnikov¡s homoclinic-saddle-focus theorem*, Journal of Differential Equations, 1993, 102(2), 305–329.